Molecular Microbiology (2013) 88(4), 673–686 ■
doi:10.1111/mmi.12201
First published online 27 March 2013

Peptidoglycan transformations during *Bacillus subtilis* sporulation

Elitza I. Tocheva,[1] Javier López-Garrido,[3] H. Velocity Hughes,[4] Jennifer Fredlund,[3] Erkin Kuru,[5] Michael S. VanNieuwenhze,[5] Yves V. Brun,[4] Kit Pogliano[3] and Grant J. Jensen[1,2]*

[1]*Division of Biology and* [2]*Howard Hughes Medical Institute, California Institute of Technology, 1200 E California Blvd., Pasadena, CA 91125, USA.*
[3]*Division of Biological Sciences, University of California at San Diego, La Jolla, California, USA.*
Departments of [4]Biology *and* [5]*Chemistry, Indiana University, Bloomington, IN 47405, USA.*

Summary

While vegetative *Bacillus subtilis* cells and mature spores are both surrounded by a thick layer of peptidoglycan (PG, a polymer of glycan strands cross-linked by peptide bridges), it has remained unclear whether PG surrounds prespores during engulfment. To clarify this issue, we generated a slender Δ*ponA* mutant that enabled high-resolution electron cryotomographic imaging. Three-dimensional reconstructions of whole cells in near-native states revealed a thin PG-like layer extending from the lateral cell wall around the prespore throughout engulfment. Cryotomography of purified sacculi and fluorescent labelling of PG in live cells confirmed that PG surrounds the prespore. The presence of PG throughout engulfment suggests new roles for PG in sporulation, including a new model for how PG synthesis might drive engulfment, and obviates the need to synthesize a PG layer *de novo* during cortex formation. In addition, it reveals that *B. subtilis* can synthesize thin, Gram-negative-like PG layers as well as its thick, archetypal Gram-positive cell wall. The continuous transformations from thick to thin and back to thick during sporulation suggest that both forms of PG have the same basic architecture (circumferential). Endopeptidase activity may be the main switch that governs whether a thin or a thick PG layer is assembled.

Accepted 4 March, 2013. *For correspondence. E-mail Jensen@caltech.edu, Tel. (+1) 626 395 8827, Fax (+1) 626 395 5730.

Introduction

The bacterial cell envelope is a complex multilayered structure (Silhavy *et al.*, 2010). It protects the cell from harsh environments, facilitates transport of molecules in and out of the cell, and is used to maintain a proton gradient. More than 100 years ago Christian Gram developed a staining procedure that classified bacterial cells into two major groups – Gram '-positive' and '-negative' – based on their ability to retain the chemical crystal violet (Gram, 1884). With the advent of electron microscopy, the fundamental structural differences between the two classes of bacteria were clarified: canonical Gram-negative bacterial cell envelopes consist of two membranes and a thin layer of peptidoglycan (PG) between them, and Gram-positive cells have one membrane surrounded by a much thicker layer of PG (Chapman and Hillier, 1953). Despite the obvious importance, many aspects of the structure and function of the cell envelope remain poorly understood.

Peptidoglycan is a large polymer that surrounds the cell. It consists of long glycan strands formed by repeating units of *N*-acetyl glucosamine-*N*-acetyl muramic acid, which are cross-linked through pentapeptide chains (Typas *et al.*, 2011). PG adds mechanical strength to the cell envelope and maintains cell shape (Thwaites and Mendelson, 1991; Tuson *et al.*, 2012). The structure of PG from Gram-negative bacteria has been extensively studied and electron cryotomography (ECT) studies showed by direct imaging that the glycan chains in *Escherichia coli* and *Caulobacter crescentus* lie parallel to the cell membrane roughly perpendicular to the long axis of the cell (an architecture that we call here 'circumferential') (Gan *et al.*, 2008). This ultrastructural analysis also indicated that the cell walls were only a single layer thick, consistent with the thin appearance of the PG in earlier cryo-sections of *E. coli* and *Pseudomonas aeruginosa* (Matias *et al.*, 2003).

Even though the PG layer of Gram-positive cells is composed of the same building blocks as Gram-negative cells, it appears much thicker in electron micrographs. It is possible that the molecular structure is similar to that of Gram-negative bacteria, but is multi-layered. In support of this idea, studies of purified sacculi from the classic Gram-positive model species *Bacillus subtilis* have already suggested circumferential orientation of the glycan strands (Verwer and Nanninga, 1976), and movements of various

components of the cell wall synthetic machinery have also been shown to be circumferential (Dominguez-Escobar *et al*., 2011; Garner *et al*., 2011). Recent literature proposes other models, however. NMR studies led to a 'scaffold' model, where the glycan strands are oriented perpendicular to the cell surface (Dmitriev *et al*., 2003). Atomic force microscopy (AFM) studies of purified *Staphylococcus aureus* sacculi showed a fibrous network with many pores (Touhami *et al*., 2004), but AFM images of purified *B. subtilis* sacculi looked quite different, and led to a 'coiled-coil' model where glycan strands are bundled together, coiled tightly to form ~ 50 nm hollow cables, and finally wrapped around cells (like a telephone cord wrapped around a barrel) (Hayhurst *et al*., 2008).

When growth conditions become unfavourable, some members of the phylum *Firmicutes* including *B. subtilis* undergo a complex morphological transformation called sporulation which has been used as a basic system to study membrane movements and cell–cell communication (Errington, 2010, Errington, 2003). Sporulation begins with the formation of an asymmetric septum that divides the cell into a smaller 'prespore' and a larger mother cell. Next, in a process similar to phagocytosis, the mother cell membranes migrate around the prespore until the engulfing membranes meet and fuse, releasing the 'forespore' into the mother cell cytoplasm. Transmission electron microscopy (TEM) images have shown that sporulation septa are formed by the inward growth of a thick disk of septal PG and cytoplasmic membrane. After septation, this thick PG layer is thinned (Holt *et al*., 1975) by sporulation-specific enzymes that degrade septal PG and then localize to the leading edges of the engulfing membranes (Abanes-De Mello *et al*., 2002; Chastanet and Losick, 2007; Gutierrez *et al*., 2010; Morlot *et al*., 2010). PG degradation is rate-limiting for membrane migration throughout engulfment (Abanes-De Mello *et al*., 2002; Gutierrez *et al*., 2010) and it has been proposed that these membrane-anchored enzymes processively degrade PG and thereby move the mother cell membranes around the prespore (Abanes-De Mello *et al*., 2002; Morlot *et al*., 2010). While it has remained unclear if these enzymes completely degrade the septal PG, TEM images have not shown any clear PG layer between the mother cell and prespore membranes during engulfment (Holt *et al*., 1975; Aronson and Fitz-James, 1976).

It has long been known that after engulfment, new PG is synthesized to produce the cortex, the thick modified PG layer that protects the spore (Tipper and Linnett, 1976; Sekiguchi *et al*., 1995; Atrih *et al*., 1998; Meador-Parton and Popham, 2000; McPherson *et al*., 2001; Vasudevan *et al*., 2007). More recently, it has been found that PG synthesis also likely occurs during engulfment. Specifically, fluorescently labelled PG precursors localize to the leading edges of engulfing membranes (Meyer *et al*., 2010). Furthermore, blocking PG synthesis with fosfomycin inhibits membrane migration in cells lacking the SpoIIQ–SpoIIIAH backup engulfment proteins and blocks engulfment membrane fission in wild type cells (Meyer *et al*., 2010). Studies of specific enzymes are complicated, however, by the redundancy of the PG biosynthetic machinery and the requirement for PG synthesis during septum formation (Buchanan and Sowell, 1983; McPherson and Popham, 2003; Korsak *et al*., 2005; Scheffers, 2005; Sauvage *et al*., 2008). The large amounts of vegetative and cortical PG present throughout and after engulfment, respectively, have also complicated searches for engulfment-specific PG (Atrih *et al*., 1996; Meador-Parton and Popham, 2000). Thus, it has remained unclear if the prespore is always surrounded by a layer of PG, or if septal PG is first completely degraded and later re-synthesized during cortex formation. More recently, ECT of whole cells and purified sacculi of an unusual *Firmicute* that is Gram-negative and produces endospores, *Acetonema longum*, showed that a layer of PG was synthesized between the prespore and mother cell membrane during engulfment (Tocheva *et al*., 2011), but it is unclear whether this also occurs in the more well-studied, Gram-positive endospore-forming bacteria.

Traditional EM preparation methods disrupt membranes and other macromolecules through cross-linking and dehydration. In contrast, ECT begins by rapidly plunge-freezing cells in their growth medium (Dubochet *et al*., 1983; Iancu *et al*., 2006), reducing specimen preparation artefacts and allowing three-dimensional images of cells to be obtained intact in a near-native state to ~ 4 nm resolution (Tocheva *et al*., 2010). To address the role of PG during engulfment in the archetypal sporulating bacterium *B. subtilis*, we generated a *ΔponA* mutant strain that was thin enough to be imaged directly with ECT. The *ponA* gene encodes for a class A penicillin-binding protein (PBP1), but previous studies have shown that since multiple PBPs exhibit redundant functions, deletion of the *ponA* gene has no significant effect on rod-shape cell morphology, cell division, sporulation, spore heat resistance, or spore germination except that cells are thinner than wild type (Popham and Setlow, 1995; Meador-Parton and Popham, 2000). Here we demonstrate that this strain is sufficiently thin for ECT, and cryotomograms of vegetative, sporulating and germinating Δ*ponA* cells reveal that a thin PG-like layer persists between engulfing membranes throughout engulfment. ECT of purified sacculi and light microscopy of fluorescently labelled PG confirm that a layer of PG persists around the prespore throughout engulfment. This layer likely serves as the foundation for assembly of the thick inner and outer cortices of the mature spore. Upon germination, the outer cortex is degraded and the inner cortex (germ cell wall) remains as the vegetative PG of outgrowing cells (Santo and Doi,

1974). *B. subtilis* therefore maintains PG around the spore continually throughout engulfment, maturation, and germination, and transforms its PG from thick to thin and back to thick. The implications of these transitions and the possible roles of PG during engulfment are discussed.

Results

ECT characterization of the ΔponA mutant

Wild type *B. subtilis* cells are typically too thick (~ 1200 nm) for high-resolution ECT imaging, so a mutation in the *ponA* gene was introduced. To test whether the PG layers of the Δ*ponA* mutant were similar to those of wild type cells, cryotomograms of Δ*ponA B. subtilis* cells were compared with the small number of lower-quality cryotomograms of wild type cells we could obtain. The cell walls of both were uniform around the cell with an average thickness of 40–50 nm (Fig. 1A and B), in good agreement with results produced with other forms of electron microscopy (Matias and Beveridge, 2005). In order to permit slightly higher resolution, sacculi from both wild type and Δ*ponA* vegetative *B. subtilis* cells were purified and imaged. The PG in both types of sacculi were again uniformly thick (40–50 nm), with smooth inner surfaces and 'fuzzy' outer surfaces (Fig. S1). High contrast, thin, planar 'patch-like' densities within the PG parallel to the membrane were occasionally observed in both wild type and Δ*ponA* cells (Fig. S1, black arrows). Unfortunately, purified sacculi from vegetative cells did not completely flatten on the EM grids due to cellular debris aggregates, limiting the resolution to less than that obtained previously for Gram-negative sacculi (Gan *et al*., 2008) (Fig. S1, white arrows).

To further characterize the Δ*ponA* mutant, dividing cells were also imaged using ECT (Fig. 1C–F) and fluorescence microscopy. On average the cells were 700 nm wide and 2 μm long. Just as in wild type *B. subtilis*, vegetative septa formed in the middle of dividing cells, ~ 2 μm from a cell pole, and exhibited symmetric ingression of the cytoplasmic membrane (Fig. 1C) with a thick layer of PG (Fig. 1D). Upon closure, the thickness of the PG in the division septum was double the thickness of the PG on the lateral cell wall (~ 80 nm, Fig. 1E), as expected as the septal PG later splits to generate two cell poles. The division septa were flat but nascent cell poles became rounder as daughter cells separated (Fig. 1E–F). The nature and transformations of the cell wall in the Δ*ponA* mutant therefore appear to mimic those of wild type cells, in keeping with the minor changes in muropeptide composition detected by mass spectrometry (Popham *et al*., 1996).

ECT of sporulating ΔponA B. subtilis

Because the Δ*ponA* cell wall resembled and behaved like that of wild type cells, and the mutant completed sporulation to nearly wild type levels (Popham and Setlow, 1995), we used it to obtain high-resolution images of sporulation. Sporulation in Δ*ponA B. subtilis* began with the formation of an asymmetrically positioned septum ~ 500 nm from one cell pole that contained PG that was roughly half the thickness of a vegetative septum (Fig. 2A). Some flat sporulation septa had only a thin layer of material continuous with and resembling PG between the inner and outer spore membranes (Fig. 2A, red dotted line in inset); presumably because these were undergoing or had already completed septal thinning. Later, the septal membranes became convex around the prespore (Fig. 2B) and migrated around the prespore toward the cell pole (Fig. 2C–D). The pole of the mother cell did not enlarge during engulfment, but rather retained its original diameter. As engulfment proceeded, the forespore also maintained its width but increased in length, as also evident in timelapse microscopy of this process (Pogliano *et al*., 1999). The thin, continuous layer of PG-like material between the inner and outer spore membranes persisted throughout engulfment, always connected to and continuous with the cell wall (Fig. 2B–D, red dotted line in insets). The distance between the inner and outer spore membranes during engulfment was ~ 22 nm (measured 'peak' to 'peak'). During engulfment, an additional layer of density was observed on the mother side of the septum (Fig. 2D) that likely represents an early assembly stage of the multilayered protein coat (Fig. 2H) (McKenney *et al*., 2012). After engulfment the forespore of the Δ*ponA B. subtilis* appeared elliptical with typical dimensions of ~ 0.6 μm × 0.9 μm, and was completely surrounded by coat material (Fig. 2E–F, arrows).

Mature spores were ellipsoidal with final dimensions of ~ 1 μm × 1.5 μm. Two thick layers of cortex were apparent between the inner and outer spore membranes. The inner cortex (germ cell wall) was denser and more uniform in thickness (~ 50–70 nm) than the outer cortex (50–100 nm). The inner and outer spore membrane and various coat layers were also clearly discernable (Fig. 2G–H inset). During germination, the outer cortex and coat were shed from the remaining inner cortex and spore (Fig. 2H–J). A thin interfacial layer of higher density was observed between the inner and outer cortex (Fig. 2J, arrows). The inner cortex appeared intact and resembled the thickness and density of vegetative PG (~ 50 nm). During outgrowth, the inner cortex remained associated with the newly emerging cells as their thick vegetative cell wall.

ECT of purified sacculi from sporulating wild type and ΔponA B. subtilis

To test whether the observed layer of PG-like material between the engulfing mother cell membrane and the prespore membrane in the cryotomograms was PG,

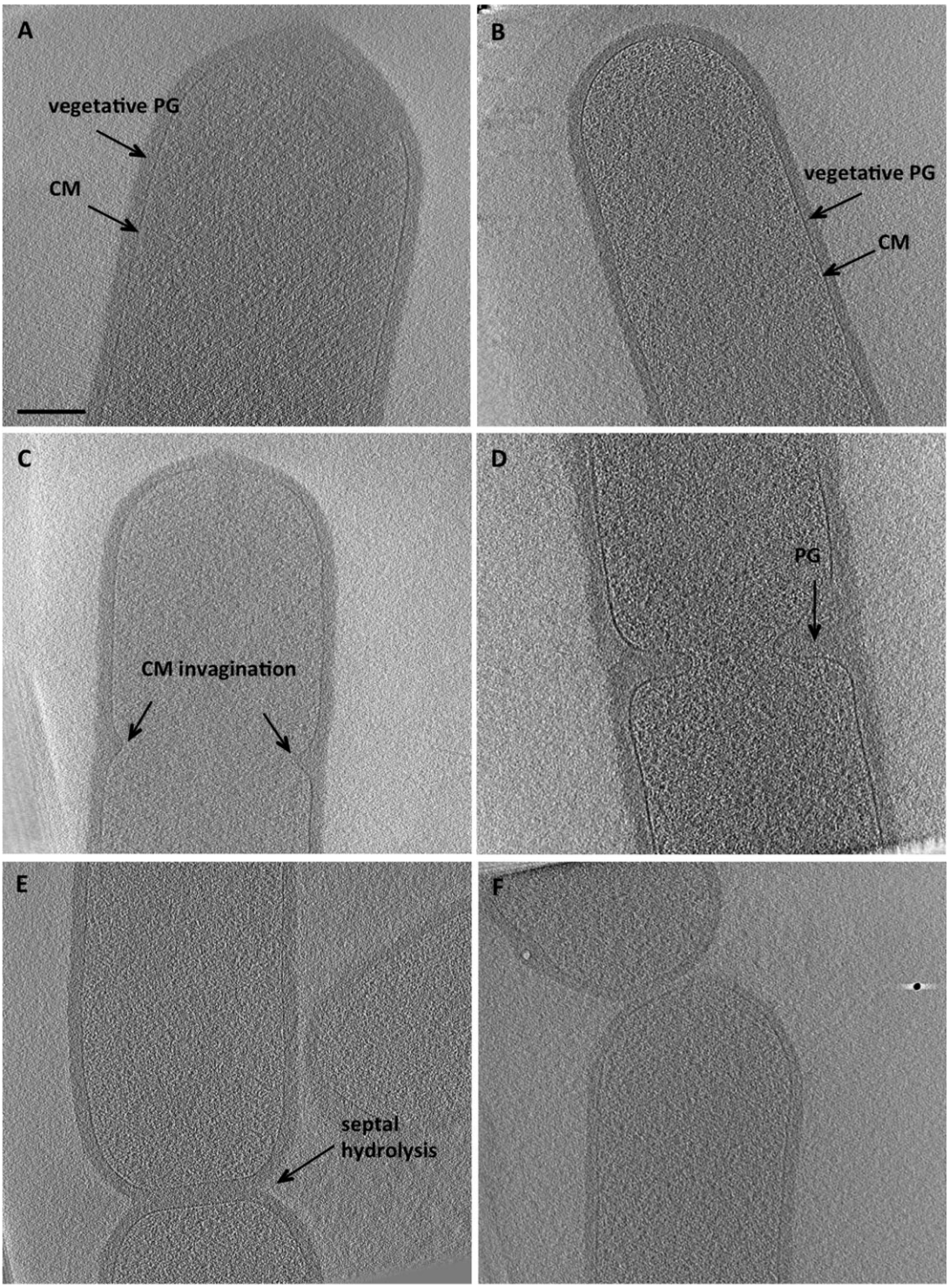

Fig. 1. Δ*ponA B. subtilis* cells undergo regular binary fission. Tomographic slices through.
A. Wild type *B. subtilis* PY79 cell with typical Gram-positive, 40–50 nm thick cell wall. PG, peptidoglycan; CM, cytoplasmic membrane.
B. Vegetative Δ*ponA B. subtilis* cell with an average cell width of ~ 700 nm also displays a typical Gram-positive cell envelope with 40- to 50-nm-thick cell wall.
C. A dividing Δ*ponA B. subtilis* cell during an early stage of vegetative septum formation.
D. A more advanced stage of vegetative septum formation in Δ*ponA B. subtilis* showing the presence of ~ 80-nm-thick PG between ingressing membranes.
E. Two Δ*ponA B. subtilis* daughter cells during septal PG hydrolysis.
F. Dividing Δ*ponA B. subtilis* cells at a final stage of binary fission. Scale bar 200 nm.

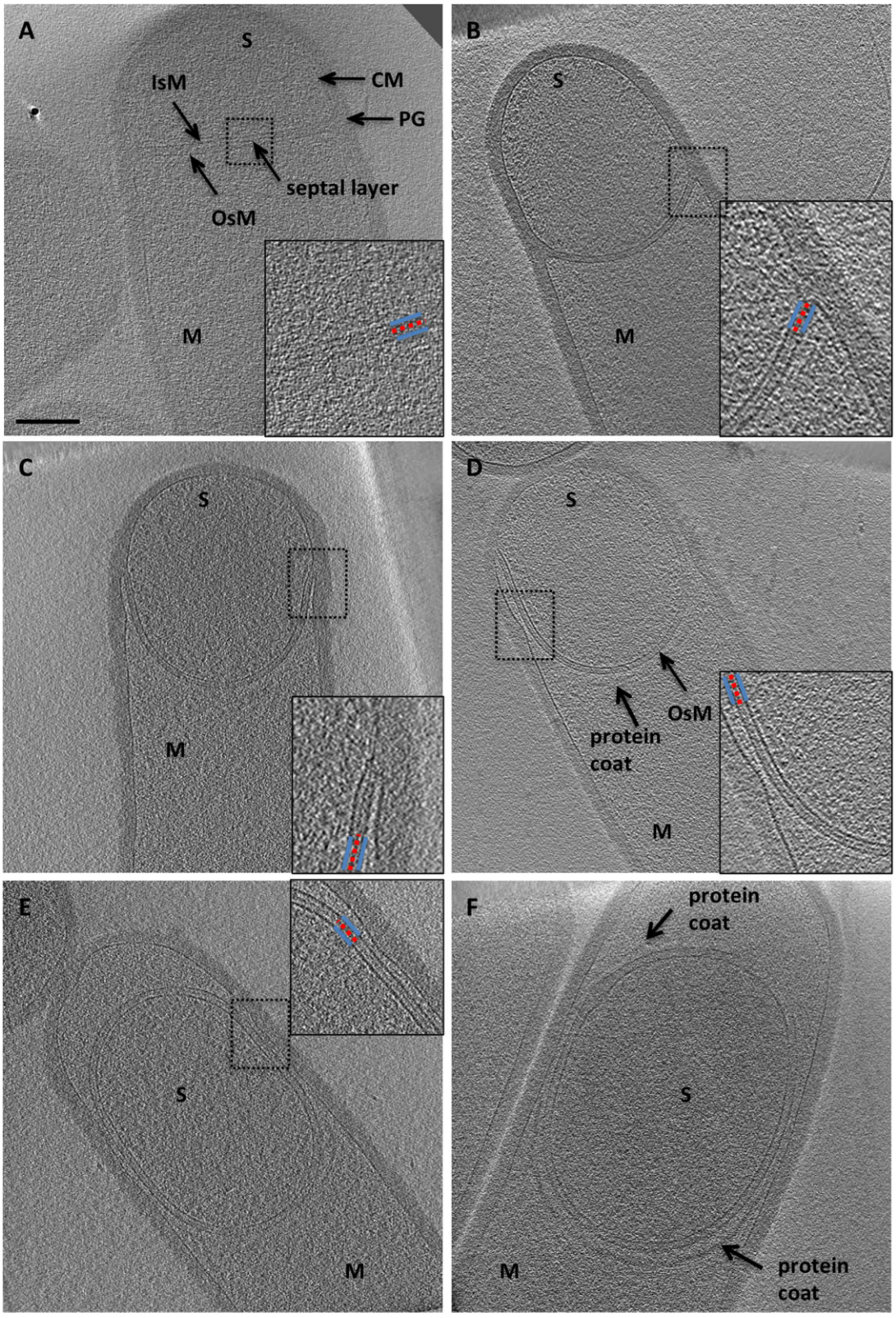
A
S
IsM
CM
PG
septal layer
OsM
M
B
S
M
C
S
M
D
S
OsM
protein
coat
M
E
S
M
F
protein
coat
S
M
protein
coat

Fig. 2. *cont.*

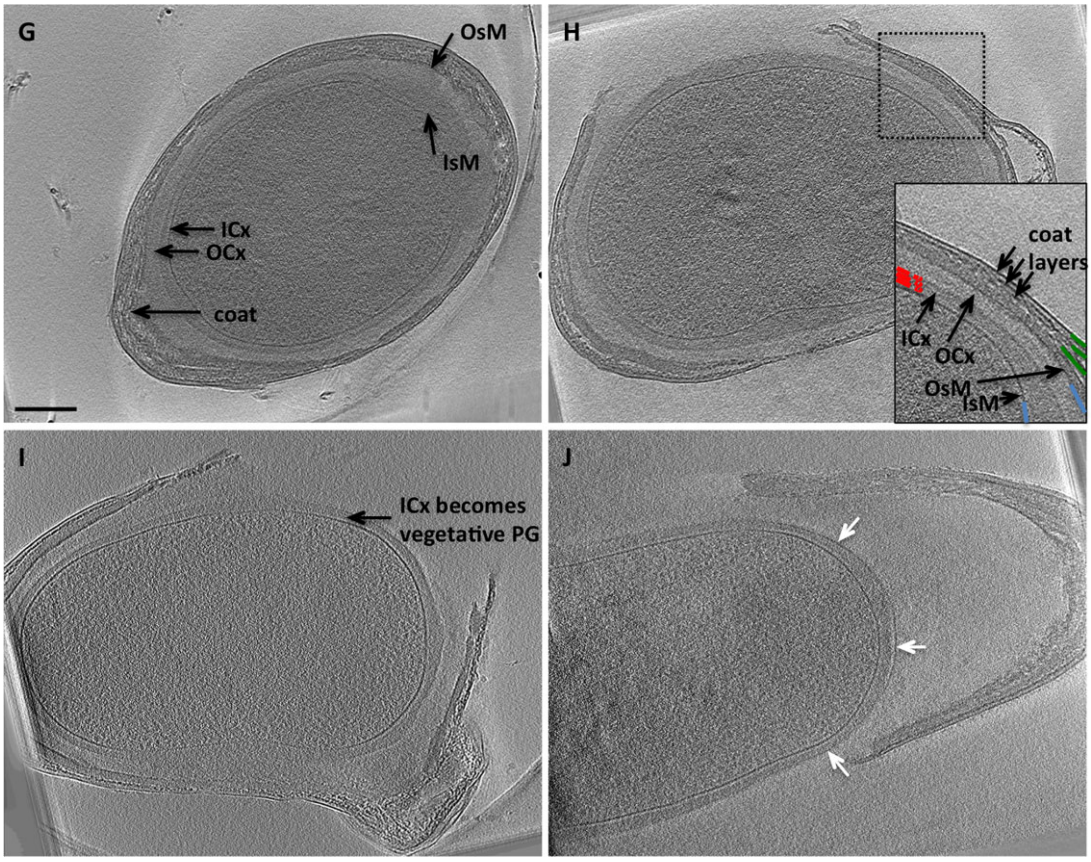

Fig. 2. ECT of sporulating and germinating Δ*ponA B. subtilis*.
A. A sporulation septum is formed by the cytoplasmic membrane (CM) and separates the prespore (S) from the mother cell (M); PG, peptidoglycan; IsM, inner spore membrane; OsM, outer spore membrane.
B. A septum after septal thinning and during early stages of engulfment.
C and D. Septa during later stages of engulfment. A protein coat assembles on the mother side of the OsM.
E. Complete engulfment.
F. Protein coat synthesis is observed all around the forespore.
Dashed boxes indicate the areas enlarged in insets. Insets show that a layer of material (red, dotted line) is retained between the IsM and OsM (solid blue lines) throughout engulfment.
G. A mature spore is ellipsoidal and is surrounded by numerous protective layers: IsM, OsM, ICx (inner cortex or germ cell wall), OCx (outer cortex) and spore coat.
H. A spore during an early stage of germination shows degradation of the OCx and opening of the coat. The inset shows the multi-layered structure of the spore coat: IsM and OsM are shown in blue, ICx is shown in red dashed lines, protein coat layers are shown in dark green.
I. A germinating spore shows that the ICx becomes the vegetative PG of outgrowing cells.
J. A spore during later stage of germination shows that the OCx and coat are shed. White arrows point to a 'layered patch' of PG in the ICx.
Scale bar 200 nm.

sacculi from wild type *B. subtilis* cells at different stages of sporulation were purified. As with sacculi from vegetative cells, some cellular debris persisted inside throughout the purification, preventing the sacculi from flattening on the EM grids. The septal PG in the sacculi of sporulating cells varied in thickness, with some appearing 40 nm thick, similar to the cell wall of the mother cell (Fig. S2A, arrows). Others showed septal PG ~ 20 nm thick at the edges and thinner in the middle (Fig. S2B), consistent with observations that septal PG degradation commences at the septal midpoint (Perez *et al*., 2000). Other sacculi showed undulating layers of very thin (~ 2 nm) septal PG that could be traced across the cell, connecting the two sides of the mother cell wall (Figs 3A and S2). Cellular debris was often seen stuck to or penetrating the middle of the thin septal PG. Late stages of engulfment were not seen, perhaps because of increased fragility.

*Fluorescent labelling of PG in sporulating wild type and Δ*dacA* B. subtilis*

In order to further confirm that a layer of PG surrounds the prespore throughout engulfment, we labelled sporulating cells with fluorescent derivatives of D-amino acids (FDAAs), which can be covalently incorporated at the fifth position of the stem peptide in PG chains, substituting for

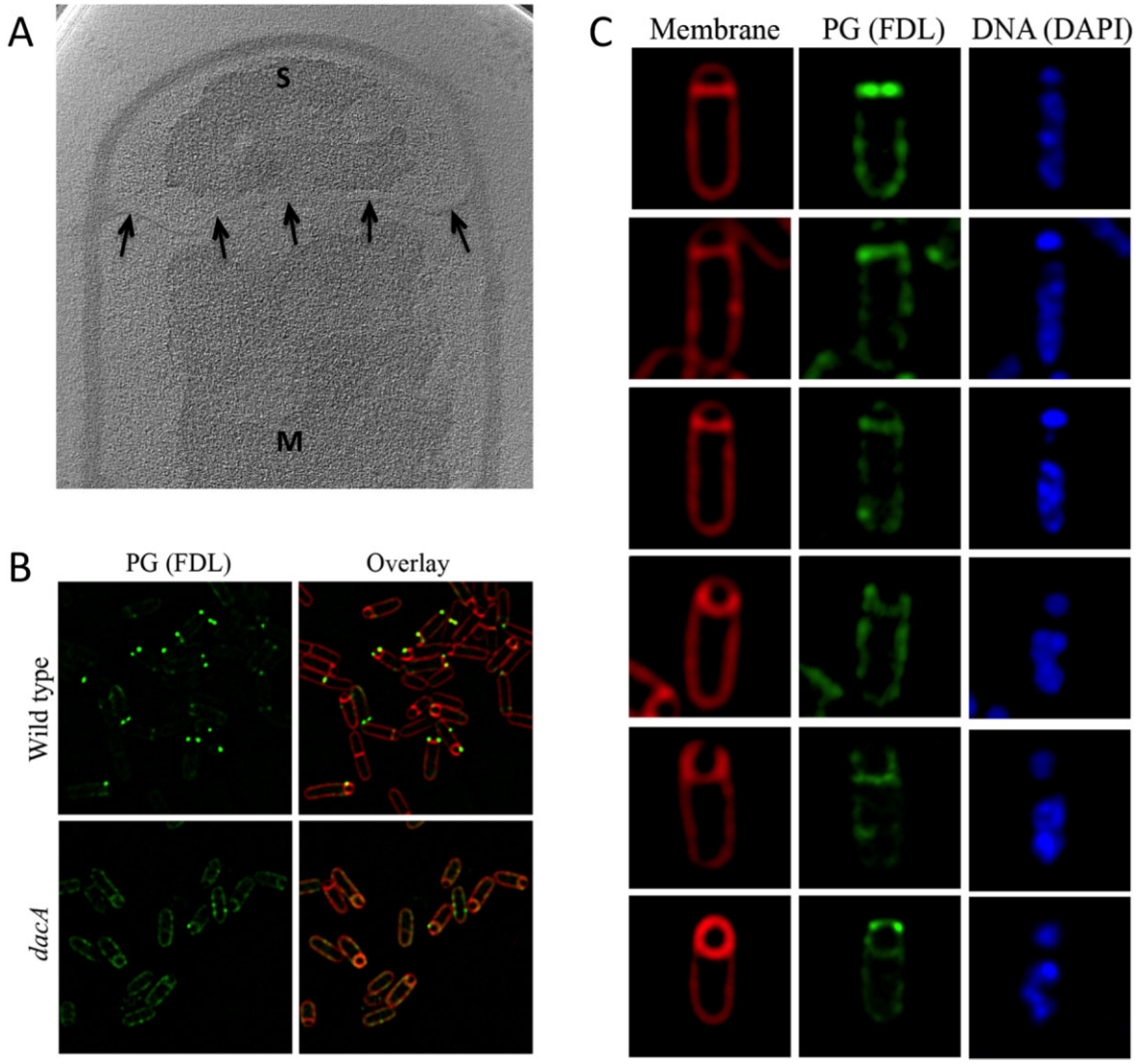

Fig. 3. Thin PG surrounds the prespore during engulfment.
A. A tomographic slice through a purified wild type *B. subtilis* sacculus showing a thin layer of PG (black arrows) connecting opposite lateral sides of the mother cell. S, spore; M, mother cell.
B. Fluorescent labelling of PG in wild type (upper panel) and Δ*dacA* (lower panel) *B. subtilis* sporulating cells stained with FDL (green). Membranes were stained with FM4-64 (red). In wild type cells, bright FDL foci are observed close to the leading edge of the engulfing membranes. However, Δ*dacA B. subtilis* sporulating cells show a continuous FDL signal throughout the engulfed region around the prespore.
C. Fluorescent labelling of PG in sporulating Δ*dacA B. subtilis* stained with FDL (green), the membrane stain FM 4–64 (red) and the DNA stain DAPI (blue). Single cells in different stages of engulfment are shown. Sporangia with flat sporulation septa show brighter FDL signals in cells with smaller prespore chromosome (upper cell) than those in which the prespore chromosome is more fully translocated. As engulfment proceeds (top to bottom), a weaker FDL signal remains associated with the engulfing membranes. Whole fields of sporulating cells stained with FDL are shown in Fig. S4B.

terminal D-alanine and labelling PG in living cells (Kuru *et al.*, 2012). We hypothesized that, if the layer of dense material observed between the inner and the outer spore membranes was PG, it would incorporate FDAAs and a continuous fluorescent signal would appear around prespores throughout engulfment in *B. subtilis*.

A fluorescein-conjugated derivative of D-lysine (FDL) (Kuru *et al.*, 2012) was used to localize PG within sporulating wild type *B. subtilis* cells. As shown in Fig. 3B (upper panel) bright FDL foci are observed near the leading edge of the engulfing membranes, consistent with the localization of PG biosynthetic intermediates which localize to this position (Meyer *et al.*, 2010). However, no signal was observed in the septal region around the prespore. Given the fact that the PG layer of interest is very thin, we considered the possibility that the sensitivity of the labelling was not high enough to detect it. Typically, the terminal D-alanine of one of the two stem peptides

forming a peptide bridge is removed in the cross-linking reaction and most of the remaining terminal D-alanine is typically removed by PBP5 (encoded by the gene *dacA*), a D,D-carboxypeptidase that cleaves the terminal D-alanine of the pentapeptides in nascent PG (Lawrence and Strominger, 1970; Todd *et al*., 1986; Atrih *et al*., 1999). Incorporation of FDAA into *B. subtilis* PG is significantly higher in Δ*dacA* mutants (Kuru *et al*., 2012), so we decided to use Δ*dacA B. subtilis* mutant to maximize labelling during engulfment. While Δ*dacA* mutants are known to exhibit normal growth, spore development, resistance and germination (Todd *et al*., 1986; Buchanan and Gustafson, 1992; Popham *et al*., 1999), cryotomograms were recorded to confirm that the cells exhibited a typical sporulation septum with the same thin layer of PG-like material between the inner and outer spore membranes (Fig. S3B–D, again with reduced resolution due to the greater thickness of otherwise wild type cells).

Sporangia of Δ*dacA B. subtilis* with flat septa showed variable FDL intensities in the septum, ranging from > 10-fold to 3-fold higher than background (Fig. S4C). This variable staining likely reflects the loss of septal PG during septal thinning, since sporangia in early stages of prespore chromosome segregation showed higher FDL staining than those in later stages (Fig. 3C) (Illing and Errington, 1991). As engulfment proceeded, the septum curved around the prespore, retaining a faint and continuous FDL signal (Fig. 3C). Cells that had completed membrane migration but not membrane fission showed a fluorescent signal all around the prespore and often contained bright foci (Fig. 3C, bottom). Similar FDL labelling patterns were observed in cells imaged with or without the membrane stain (Fig. S5A) but not in cells incubated with free fluorescein (Fig. S5B), suggesting that the staining was in fact the result of FDL incorporation in PG chains. Altogether, FDL staining of sporulating wild type and Δ*dacA B. subtilis* cells suggests that, although PG may be actively synthesized at the leading edge of the engulfing membrane, a layer of PG is continuously present between the mother cell and prespore membranes throughout engulfment.

Discussion

A thin layer of PG surrounds prespores throughout engulfment

Exploiting a slender *B. subtilis* mutant amenable to high-resolution ECT, here we have shown that a thin layer of material continuous with and resembling the cell wall surrounds prespores throughout engulfment. This thin layer was likely missed in previous EM studies (Holt *et al*., 1975; Aronson and Fitz-James, 1976; Illing and Errington, 1991) because of the fixation, plastic embedding, sectioning and staining inherent in traditional approaches (Matias and Beveridge, 2005). ECT of purified wild type sacculi during sporulation and direct fluorescent labelling of PG in live cells confirmed that the observed thin layer was in fact PG (Figs 3, S2 and S4).

The presence of a thin PG between engulfing membranes in *B. subtilis* could be due to one of the following two possibilities: (1) an innermost layer of PG is separated from the thick mother PG and directed into the septum, or (2) a new, thin layer of PG is synthesized at the leading edge of the engulfing membranes. Comparison of the PG transformations in *B. subtilis* and *A. longum* allows us to distinguish between these two possibilities. In *A. longum*, the vegetative cell wall is only a layer thick and follows the membranes into the sporulation septum. The single layer of PG observed between the engulfing membranes, therefore, must be newly synthesized. Because the PG synthetic machinery of these two species are so similar, *B. subtilis* likely also synthesizes a thin layer of PG during engulfment. Furthermore, fluorescent labelling of wild type and Δ*dacA B. subtilis* show different labelling patterns, indicating that the septal PG layer is modified by PBPs similarly to the vegetative cell wall. The incorporation of FDAA therefore labels newly synthesized PG. Lastly, the PG just ahead of the engulfing membranes (Fig. 4B, black arrow) is thicker than just behind (white arrow), and the PG behind the junction is not thinner than the rest of the cell wall, all consistent with synthesis of new, additional PG at the leading edge of the junction rather than separation of existing PG (Fig. 4B).

These observations suggest three potential functions of the thin layer of PG during engulfment. First, it may provide mechanical strength as the genome is packed within the prespore. Second, PG synthesis may drive membrane movement during engulfment. Third, it may serve as a template for elaboration of the cortex. Concerning membrane movement, immediately after septal thinning, the thin layer of PG between the septal membranes is flat. During engulfment, the septum becomes convex and then the perimeter migrates towards the cell pole. As suggested previously (Lopez-Diaz *et al*., 1986; Smith *et al*., 1993; Frandsen and Stragier, 1995), septal thinning might be required to give the septum enough flexibility to undergo these morphological changes. The hydrolytic enzymes that mediate septal thinning are also rate limiting for membrane migration and it has been further proposed that they move the membranes around the prespore by a burnt-bridge ratchet mechanism, pulling the membrane towards the pole by binding and hydrolysing glycan strands along the path (Abanes-De Mello *et al*., 2002; Gutierrez *et al*., 2010; Morlot *et al*., 2010). The results described here demonstrate that septal curving and membrane migration towards the cell pole must also require PG *synthesis*, since the septal PG must cover an increasingly large surface. This rationalizes why fluores-

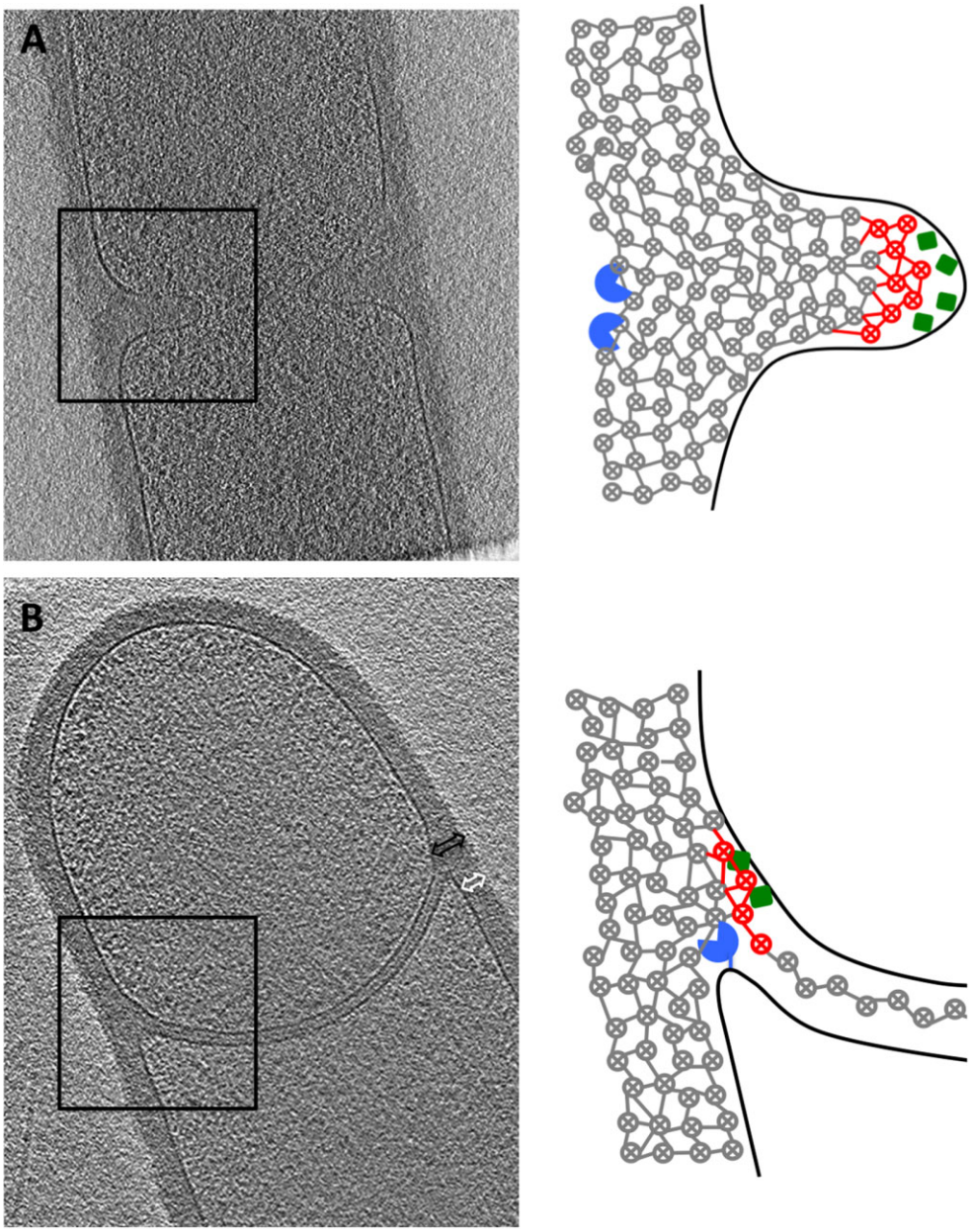

Fig. 4. A model for PG hydrolysis and synthesis during (A) vegetative septation and (B) engulfment. Schematics represent the boxed areas in the tomographic slices. Membranes are shown in black, glycan strands are viewed end-on (circled X's) interconnected by peptide bonds (lines). Older glycan strands and cross-links are shown in grey, new glycan strands and cross-links are shown in red, PG synthases are green and PG hydrolases are blue. During vegetative septation, new PG synthesis is thought to push the cytoplasmic membrane towards the middle of the cell. Hydrolysis occurs after septation from the outside. Similarly, we propose that during engulfment, co-ordinated PG synthesis at the 'front' and hydrolysis at the 'back' of the septal junction may drive membrane migration towards the pole. Black arrow indicates PG synthesis, white arrow points to average thickness of vegetative cell wall.

cently labelled PG building blocks were observed localizing at the leading edge of the engulfing membrane (Meyer *et al*., 2010). Moreover, because synthesis of new PG is known to drive cell shape changes (such as division (Cabeen and Jacobs-Wagner, 2005)) and move PG synthetic enzymes across membranes (Dominguez-Escobar *et al*., 2011; Garner *et al*., 2011), we suggest that synthesis of the thin layer of septal PG may help drive engulfment (Meyer *et al*., 2010). Specifically, addition of new glycan strands at the front (pole-facing) side of the junction between the septal PG and the cell wall may push the inner spore membrane inward, and create new cross-links with the cell wall in front of the junction (Fig. 4B, red strands). Hydrolysis at the back (mother-cell-facing) side

of the junction may cleave older cross-links, freeing the trailing surface of the growing septal PG from the cell wall. PG-synthetic enzymes could be localized to the front face by expression in the prespore (Fig. 4, green squares). PG-degrading enzymes could be localized to the back face by expression in the mother cell (Fig. 4, blue circles). As the cross-links between the septal PG and the cell wall are released on the back of the junction, the outer spore membrane could explore the newly empty space by Brownian motion and be captured in an advanced position by membrane-embedded proteins that bind to PG. Thus co-ordinated PG synthesis and hydrolysis could gradually move the sporulation septum towards the pole.

Sporulating bacteria go through both 'Gram-positive' and 'Gram-negative' phases

The growth of the thin septal PG suggests that in addition to its thick, archetypal Gram-positive cell wall, *B. subtilis* can also synthesize thin layers of PG. Moreover, *B. subtilis* interconverts the two forms: the thick cell wall is gradually thinned within the nascent sporulation septum, and the thin layer is later elaborated into the thick cortices that surround the mature spore. Upon germination, the inner spore cortex becomes the cell wall of the vegetative cell. These are the same PG transformations that were seen previously in the sporulating Gram-negative *Firmicute A. longum* (Tocheva *et al*., 2011): both *A. longum* and *B. subtilis* transform thick PG layers into thin PG layers that eventually surround the forespore and are later elaborated into a thick cortex. The only difference is the timing of the PG transformations: whereas in *B. subtilis*, the thick septal PG thins at the beginning of sporulation and then the thick inner cortex remains during germination, in *A. longum*, the thick cortical PG is thinned during germination, remaining thin during spore outgrowth, vegetative growth, and into the next sporulation cycle (Fig. 5).

As a clearly Gram-negative species, *A. longum* showed that the thin septal PG is 'Gram-negative' since it was physically continuous with its Gram-negative vegetative cell wall (Tocheva *et al*., 2011). As the archetypal Gram-positive species, *B. subtilis* shows that the thick inner spore cortex can be considered 'Gram-positive', since it becomes the cell wall during germination. Thus assuming the homologous genes in the two organisms are synthesizing PG layers with similar architectures (Vollmer *et al*., 2008), both *B. subtilis* and *A. longum* go through thin, 'Gram-negative' and thick, 'Gram-positive' phases. Both species can synthesize both forms of PG, and the two are furthermore gradually interconverted. The difference between the species is that the vegetative *B. subtilis* cells emerge in the thick, 'Gram-positive' phase and vegetative *A. longum* cells emerge in the thin, 'Gram-negative' phase, following germination. Our observation that in both species, spores and cells appear to be continuously surrounded by PG throughout their development, suggests that *de novo* untemplated synthesis of new PG layers is not necessary.

Similar to thin PG, thick PG is likely 'circumferential'

As explained in the Introduction, there are currently three models for the architecture of Gram-positive PG: scaffold, coiled-coil, and circumferential. Our observation that the thick PG in the *B. subtilis* sporulation septum is gradually thinned to a thin, Gram-negative-like layer argues strongly against the coiled-coil model, since it is unclear how 50 nm coils could be 'thinned' by hydrolysis to just ~ 2 nm thick without jeopardizing the integrity of the cable. It is nicely consistent, however, with the possibility that the architecture of Gram-positive PG is basically the same as Gram-negative (circumferential), differing only in the number of layers, since such related forms could be gradually interconverted. The coiled-coil model also predicts that the Gram-positive cell wall should appear as a row of hollow tubes, but in our cryotomograms of wild type, Δ*ponA* and Δ*dacA B. subtilis* cells it appeared flat and almost uniformly dense, without any indication of cables or coils (Figs 1 and S3). The only deviations from uniform density were a few planar patches of high density observed within the cell wall parallel to its faces. These were seen in whole cells, purified sacculi of wild type and Δ*ponA B. subtilis*, and in mature spores (Figs 1–2 and Fig. S1). Since sacculi lack proteins, these patches are likely PG, and therefore further support the circumferential model. The patches were more prominent at the cell poles, in the Δ*ponA* mutant, and at the interface between the inner and outer cortex. Since these are all places reported to experience slower growth (Popham and Setlow, 1996; de Pedro *et al*., 1997), patches may reflect variations in packing density. Through ECT of purified sacculi and multi-scale computational modelling, Beeby *et al*. provide additional evidence that like Gram-negative PG, the architecture of Gram-positive PG is neither scaffold nor coiled-coil, but rather circumferential (see companion article in this issue – Beeby *et al*., 2013).

Mechanistic implications for cell wall synthesis

The current model for PG synthesis in Gram-positive bacteria is that while new material is inserted on the inner face of the cell wall, old material is removed on the outside by autolysins, resulting in 'inside-to-out' growth (Holtje and Glauner, 1990). Given the evidence presented here and by Beeby *et al*. that the basic architecture of Gram-positive and Gram-negative PG is the same (circumferential), and the numerous biochemical and genetic studies that have shown that the enzymes responsible

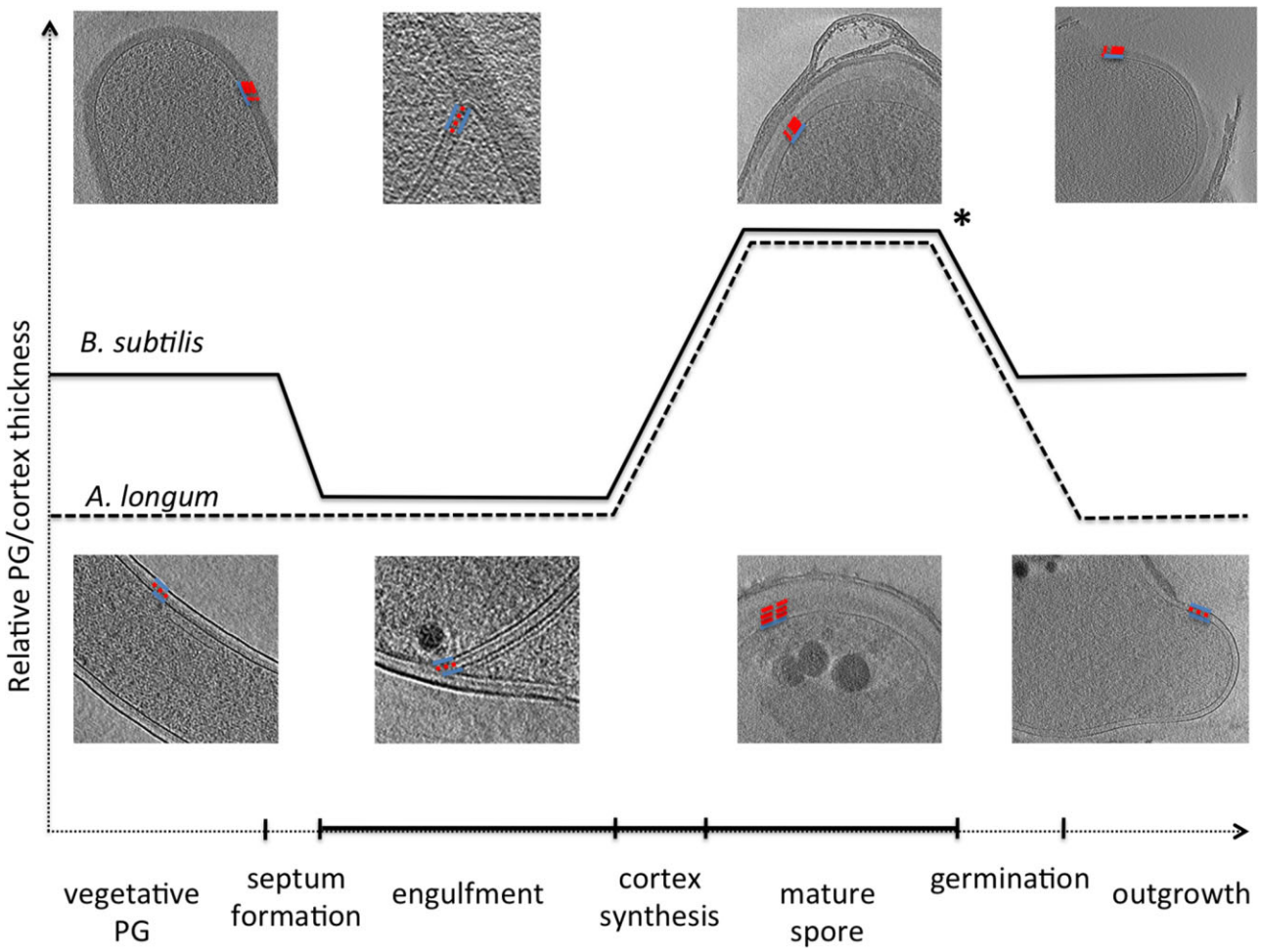

Fig. 5. Continuous PG and cortex model during sporulation in *A. longum* (dashed line) and *B. subtilis* (solid line). The Gram-negative *A. longum* synthesizes a thin layer of PG during vegetative growth and engulfment. During spore maturation, the thin PG is elaborated into a thick cortex which gets degraded back to thin PG during outgrowth. *B. subtilis* has a thick cell wall during vegetative growth, which thins during engulfment. The thin PG is elaborated into a thick cortex during spore maturation and remains thick during outgrowth (where the ICx becomes the vegetative PG). The two cells overlap in their PG/cortex morphologies during engulfment and spore maturation and the major mechanistic difference between the two cell types likely occurs upon germination (asterisk). Tomographic slices from *B. subtilis* (top) and *A. longum* (bottom) cells at different stages of sporulation represent the major PG transformations. PG is marked as dotted red line and membranes are traced as solid blue lines.

for synthesizing PG in Gram-negative and Gram-positive species are highly homologous (McPherson *et al.*, 2001; Foster and Popham, 2002; Sauvage *et al.*, 2008) and redundant (Sauvage *et al.*, 2008), it is possible that the main difference in their assembly is as simple as turning on or off a peptidase: if existing peptides are not cleaved, new layers of glycan strands must accumulate inside of old layers, resulting in thick, Gram-positive PG. If, however, existing peptides are cleaved as new glycan strands are added, the existing layer will split and incorporate the new strands, resulting in thin, Gram-negative PG. Of course another major difference between Gram-negative and Gram-positive PG is the presence of teichoic acids. Other differences include slight modifications in the peptide composition, the degree of peptide cross-links, and the length of the PG chains (Vollmer *et al.*, 2008). It is interesting to note that since the periplasmic space of Gram-negative bacteria structurally mimics the inter-membrane space of the sporulation septum (two membranes separated by a thin layer of PG), it is possible that this physical constraint drives the initial synthesis of thin PG in both situations.

Experimental procedures

Construction of the ΔponA B. subtilis *mutant*

DNA regions upstream and downstream of *ponA* coding sequence in *B. subtilis* PY79 were amplified with the following primers: Forward primer: 5′-ggaattcctgtctctcacggagtc caag-3′ (EcoRI restriction site underlined) and Reverse

primer: 5′-cgcggatccgatctgacataacatctcaacctttcg-3′ (BamHI restriction site underlined) resulting in a 939 bp fragment. The downstream region of the *ponA* gene was amplified with the Forward primer: 5′-aataatctcgaggaatgattcaacaggttctgac acga-3′ (XhoI restriction site underlined) and Reverse primer: 5′-aataatgcatgcttgaagattacggcggagaagtg-3′ (SphI restriction site underlined) which resulted in a 1052 bp fragment. The upstream and downstream DNA fragments were digested with EcoRI–BamHI and XhoI–SphI respectively, and subsequently cloned in pEB71 (a pUC plasmid derivative with *loxP* sites flanking a Kan^R cassette). Naturally competent *B. subtilis* PY79 cells were transformed with the resulting plasmid and selected for with kanamycin. The construct was confirmed by PCR using the following primers: Forward: 5′-ccagttcgctctttcataggct-3′ and Reverse: 5′-gagcttcagcaggat attaaatcaatcg-3′.

Culture growth and sample preparation

Wild type *B. subtilis*, Δ*ponA* and Δ*dacA* (Kuru *et al*., 2012) mutant cells were grown in LB for vegetative growth and germination. Sporulation was induced by resuspension as previously described (Becker and Pogliano, 2007). Briefly, cells were grown to OD_{600} = 0.5–0.7 in ¼ diluted LB at 37°C. Cells were spun down at 3000 *g* for 5 min, resuspended in sporulation medium and incubated at 37°C with shaking. One litre of sporulation medium contains 1 ml of 3 μM $FeCl_3$•$6H_2O$, 40 μM $MgCl_2$•$6H_2O$, 38 μM $MnCl_2$•$4H_2O$; 10 ml of 1 M NH_4Cl, 75 mM Na_2SO_4, 0.12 M NH_4NO_3, 0.05 M KH_2PO_4, 50 ml of 0.5 M MOPS pH 7.5, 2 ml of 10% glutamic acid, 1 ml 0.1 M $CaCl_2$, 4 ml 1 M $MgSO_4$. Cells were grown in sporulation medium for 1.5 h to observe septum formation, 2–3 h to observe engulfment and 4–5 h for engulfment completion. Mature spores were purified as described previously (Tocheva *et al*., 2011).

Sacculi purification

Sacculi from vegetative Δ*ponA* and wild type *B. subtilis* were purified as described previously (Tocheva *et al*., 2011). To minimize the cellular debris in sacculi from sporulating wild type *B. subtilis* the following optimized procedure was used. Cells were grown as described above. After 2.5 h of growth in sporulation medium cells were washed in cold 50 mM Tris, pH 7.5 and resuspended in 4% SDS. The cells were then shaken at 150 rpm at 30°C for 2 h and subsequently sonicated 5× for 30 s at 50% amplitude. After sonication, the cells were boiled in a water bath for 1 h and centrifuged at 37 000 *g* at room temperature. The cells were washed once with 0.1% Triton X-100 and 5× with H_2O. The sacculi were treated with DNase, RNase and peptidases to remove remaining respective macromolecules. Teichoic acids were not removed from either Δ*ponA* or wild type *B. subtilis* sacculi since their removal destroys the cellular shape and rigidity of the sacculi (Matias and Beveridge, 2005).

ECT data collection and processing

Tilt-series of vegetative, sporulating and germinating Δ*ponA B. subtilis* cells, purified sacculi of wild type and Δ*ponA B. subtilis*, mature spores of Δ*ponA B. subtilis* and sporulating Δ*dacA B. subtilis* were collected with an FEI Polara (FEI Company, Hillsboro, OR) 300 kV FEG transmission electron microscope equipped with a Gatan energy filter and a lens-coupled 4k × 4k UltraCam or K2 Summit™ counting direct detector camera (Gatan, Pleasanton, CA). Data were collected with Leginon (Suloway *et al*., 2005) or UCSFTomo (Zheng *et al*., 2007). The tomograms were obtained by using 22.5 × K magnification, 10 μm defocus, 120–200 electrons per $Å^2$ total dose, ± 65° total tilt, and 1° increments. Three-dimensional reconstructions were calculated with IMOD using the weighted back-projection method (Kremer *et al*., 1996).

Fluorescence microscopy and image analysis

Fluorescently labelled amino acids were recently developed and successfully incorporated in vegetative PG of wild type and Δ*dacA B. subtilis* at position 5 of the muramyl pentapeptide (Cava *et al*., 2011). In order to visualize the presence of newly synthesized PG between mother cell and prespore membranes we first labelled wild type *B. subtilis* cells with FDL, a fluorescein-conjugated derivative of D-lysine. To increase the number of PG sites to be labelled during sporulation we next used Δ*dacA B. subtilis* cells and labelled them with FDL similarly to wild type. Briefly, cells were induced for sporulation as described above. Samples were collected 1.5 and 2.5 h after resuspension in sporulation medium, incubated with 500 μM FDL or non-conjugated fluorescein for 5 min and washed 3 times with sporulation medium. The cells were then added to agarose pads supplemented with 1 μg ml^{-1} FM 4–64 for membrane visualization and 40 ng ml^{-1} DAPI for chromosome visualization. Images were collected using an Applied Precision Spectris optical sectioning microscope equipped with a Photometrix CoolsnapHQ charge coupled device camera. Exposure times were 0.3–0.4 s for visualizing FDL, 0.1–0.3 s for FM 4–64 and 0.1–0.3 for DAPI. Images were deconvolved with SoftWoRx software (Applied Precision, Inc.). FDL-specific fluorescence in the sporulation septum was quantified for cells in different stages of engulfment. Net septal fluorescence of FDL treated cells was made relative to the septal fluorescence of cells in the same sporulation stage, but not treated with FDL. The resulting values (corrected fluorescence intensity) were plotted for cells in different stages. The background value is the relative septal fluorescence of cells not treated with FDL, and corresponds to 1 in every case. Fluorescence values above the background are considered to be the FDL signal.

Acknowledgements

We thank Poochit Nonejuie for the construction of Δ*ponA B. subtilis* mutant, and Dr Tim Baker and Norm Olsen for training J.F. in microscopy. This work was supported by the Howard Hughes Medical Foundation, gifts to Caltech from the Gordon and Betty Moore Foundation (to G.J.J.), GM57045 (to K.P.), AI059327 (to M.S.V.) and GM051986 (to Y.V.B.).

References

Abanes-De Mello, A., Sun, Y.L., Aung, S., and Pogliano, K. (2002) A cytoskeleton-like role for the bacterial cell wall during engulfment of the *Bacillus subtilis* forespore. *Genes Dev* **16:** 3253–3264.

Aronson, A.I., and Fitz-James, P. (1976) Structure and mor-

phogenesis of the bacterial spore coat. *Bacteriol Rev* **40:** 360–402.
Atrih, A., Zollner, P., Allmaier, G., and Foster, S.J. (1996) Structural analysis of *Bacillus subtilis* 168 endospore peptidoglycan and its role during differentiation. *J Bacteriol* **178:** 6173–6183.
Atrih, A., Zollner, P., Allmaier, G., Williamson, M.P., and Foster, S.J. (1998) Peptidoglycan structural dynamics during germination of *Bacillus subtilis* 168 endospores. *J Bacteriol* **180:** 4603–4612.
Atrih, A., Bacher, G., Allmaier, G., Williamson, M., and Foster, S.J. (1999) Analysis of peptidoglycan structure from vegetative cells of *Bacillus subtilis* 168 and role of PBP 5 in peptidoglycan maturation. *J Bacteriol* **181:** 3956–3966.
Becker, E., and Pogliano, K. (2007) Cell-specific SpoIIIE assembly and DNA translocation polarity are dictated by chromosome orientation. *Mol Microbiol* **66:** 1066–1079.
Beeby, M., Gumbart, J.C., Roux, B., and Jensen, G.J. (2013) Architecture and assembly of the Gram-positive cell wall. *Mol Microbiol* **88:** 664–672.
Buchanan, C.E., and Gustafson, A. (1992) Mutagenesis and mapping of the gene for a sporulation-specific penicillin-binding protein in *Bacillus subtilis*. *J Bacteriol* **174:** 5430–5435.
Buchanan, C.E., and Sowell, M.O. (1983) Stability and synthesis of the penicillin-binding proteins during sporulation. *J Bacteriol* **156:** 545–551.
Cabeen, M.T., and Jacobs-Wagner, C. (2005) Bacterial cell shape. *Nat Rev Microbiol* **3:** 601–610.
Cava, F., de Pedro, M.A., Lam, H., Davis, B.M., and Waldor, M.K. (2011) Distinct pathways for modification of the bacterial cell wall by non-canonical D-amino acids. *EMBO J* **30:** 3442–3453.
Chapman, G.B., and Hillier, J. (1953) Electron microscopy of ultra-thin sections of bacteria I. Cellular division in *Bacillus cereus*. *J Bacteriol* **66:** 362–373.
Chastanet, A., and Losick, R. (2007) Engulfment during sporulation in *Bacillus subtilis* is governed by a multiprotein complex containing tandemly acting autolysins. *Mol Microbiol* **64:** 139–152.
Dmitriev, B.A., Toukach, F.V., Schaper, K.J., Holst, O., Rietschel, E.T., and Ehlers, S. (2003) Tertiary structure of bacterial murein: the scaffold model. *J Bacteriol* **185:** 3458–3468.
Dominguez-Escobar, J., Chastanet, A., Crevenna, A.H., Fromion, V., Wedlich-Soldner, R., and Carballido-Lopez, R. (2011) Processive movement of MreB-associated cell wall biosynthetic complexes in bacteria. *Science* **333:** 225–228.
Dubochet, J., McDowall, A.W., Menge, B., Schmid, E.N., and Lickfeld, K.G. (1983) Electron microscopy of frozen-hydrated bacteria. *J Bacteriol* **155:** 381–390.
Errington, J. (2003) Regulation of endospore formation in *Bacillus subtilis*. *Nat Rev Microbiol* **1:** 117–126.
Errington, J. (2010) From spores to antibiotics via the cell cycle. *Microbiology* **156:** 1–13.
Foster, S., and Popham, D. (2002) Structure and synthesis of cell wall, spore cortex, teichoic acids, S-layers, and capsules. In Bacillus Subtilis *and Its Close Relatives: From Genes to Cells*. Sonenshein, A.L., Hoch, J.A., and Losick, R. (eds). Washington, DC: American Society for Microbiology, pp. 21–41.
Frandsen, N., and Stragier, P. (1995) Identification and characterization of the *Bacillus subtilis spoIIP* locus. *J Bacteriol* **177:** 716–722.
Gan, L., Chen, S., and Jensen, G.J. (2008) Molecular organization of Gram-negative peptidoglycan. *Proc Natl Acad Sci USA* **105:** 18953–18957.
Garner, E.C., Bernard, R., Wang, W., Zhuang, X., Rudner, D.Z., and Mitchison, T. (2011) Coupled, circumferential motions of the cell wall synthesis machinery and MreB filaments in *B. subtilis*. *Science* **333:** 222–225.
Gram, C. (1884) Ueber die isolirte Firbung der Schizomyceten iu Schnitt-und Trockenpriparate. *Fortschitte Medicin* **2:** 185–189.
Gutierrez, J., Smith, R., and Pogliano, K. (2010) SpoIID peptidoglycan hydrolase activity is required throughout engulfment during *Bacillus subtilis* sporulation. *J Bacteriol* **192:** 3174–3186.
Hayhurst, E.J., Kailas, L., Hobbs, J.K., and Foster, S.J. (2008) Cell wall peptidoglycan architecture in *Bacillus subtilis*. *Proc Natl Acad Sci USA* **105:** 14603–14608.
Holt, S.C., Gauther, J.J., and Tipper, D.J. (1975) Ultrastructural studies of sporulation in *Bacillus sphaericus*. *J Bacteriol* **122:** 1322–1338.
Holtje, J.V., and Glauner, B. (1990) Structure and metabolism of the murein sacculus. *Res Microbiol* **141:** 75–89.
Iancu, C.V., Tivol, W.F., Schooler, J.B., Dias, D.P., Henderson, G.P., Murphy, G.E., *et al*. (2006) Electron cryotomography sample preparation using the Vitrobot. *Nat Protocols* **1:** 2813–2819.
Illing, N., and Errington, J. (1991) Genetic regulation of morphogenesis in *Bacillus subtilis*: roles of sigma E and sigma F in prespore engulfment. *J Bacteriol* **173:** 3159–3169.
Korsak, D., Liebscher, S., and Vollmer, W. (2005) Susceptibility to antibiotics and beta-lactamase induction in murein hydrolase mutants of *Escherichia coli*. *Antimicrob Agents Chemother* **49:** 1404–1409.
Kremer, J.R., Mastronarde, D.N., and McIntosh, J.R. (1996) Computer visualization of three-dimensional image data using IMOD. *J Struct Biol* **116:** 71–76.
Kuru, E., Hughes, H.V., Brown, P.J., Hall, E., Tekkam, S., Cava, F., *et al*. (2012) In situ probing of newly synthesized peptidoglycan in live bacteria with fluorescent D-amino acids. *Angew Chem Int Ed Engl* **51:** 12519–12523.
Lawrence, P.J., and Strominger, J.L. (1970) Biosynthesis of the peptidoglycan of bacterial cell walls. XVI. The reversible fixation of radioactive penicillin G to the D-alanine carboxypeptidase of *Bacillus subtilis*. *J Biol Chem* **245:** 3660–3666.
Lopez-Diaz, I., Clarke, S., and Mandelstam, J. (1986) *spoIID* operon of *Bacillus subtilis*: cloning and sequence. *J Gen Microbiol* **132:** 341–354.
McKenney, P.T., Driks, A., and Eichenberger, P. (2012) The *Bacillus subtilis* endospore: assembly and functions of the multilayered coat. *Nat Rev Microbiol* **11:** 33–44.
McPherson, D.C., and Popham, D.L. (2003) Peptidoglycan synthesis in the absence of class A penicillin-binding proteins in *Bacillus subtilis*. *J Bacteriol* **185:** 1423–1431.
McPherson, D.C., Driks, A., and Popham, D.L. (2001) Two

class A high-molecular-weight penicillin-binding proteins of *Bacillus subtilis* play redundant roles in sporulation. *J Bacteriol* **183:** 6046–6053.
Matias, V.R., and Beveridge, T.J. (2005) Cryo-electron microscopy reveals native polymeric cell wall structure in *Bacillus subtilis* 168 and the existence of a periplasmic space. *Mol Microbiol* **56:** 240–251.
Matias, V.R., Al-Amoudi, A., Dubochet, J., and Beveridge, T.J. (2003) Cryo-transmission electron microscopy of frozen-hydrated sections of *Escherichia coli* and *Pseudomonas aeruginosa*. *J Bacteriol* **185:** 6112–6118.
Meador-Parton, J., and Popham, D.L. (2000) Structural analysis of *Bacillus subtilis* spore peptidoglycan during sporulation. *J Bacteriol* **182:** 4491–4499.
Meyer, P., Gutierrez, J., Pogliano, K., and Dworkin, J. (2010) Cell wall synthesis is necessary for membrane dynamics during sporulation of *Bacillus subtilis*. *Mol Microbiol* **76:** 956–970.
Morlot, C., Uehara, T., Marquis, K.A., Bernhardt, T.G., and Rudner, D.Z. (2010) A highly coordinated cell wall degradation machine governs spore morphogenesis in *Bacillus subtilis*. *Genes Dev* **24:** 411–422.
de Pedro, M.A., Quintela, J.C., Holtje, J.V., and Schwarz, H. (1997) Murein segregation in *Escherichia coli*. *J Bacteriol* **179:** 2823–2834.
Perez, A.R., Abanes-De Mello, A., and Pogliano, K. (2000) SpoIIB localizes to active sites of septal biogenesis and spatially regulates septal thinning during engulfment in *Bacillus subtilis*. *J Bacteriol* **182:** 1096–1108.
Pogliano, J., Osborne, N., Sharp, M.D., Abanes-De Mello, A., Perez, A., Sun, Y.L., and Pogliano, K. (1999) A vital stain for studying membrane dynamics in bacteria: a novel mechanism controlling septation during *Bacillus subtilis* sporulation. *Mol Microbiol* **31:** 1149–1159.
Popham, D.L., and Setlow, P. (1995) Cloning, nucleotide sequence, and mutagenesis of the *Bacillus subtilis ponA* operon, which codes for penicillin-binding protein (PBP) 1 and a PBP-related factor. *J Bacteriol* **177:** 326–335.
Popham, D.L., and Setlow, P. (1996) Phenotypes of *Bacillus subtilis* mutants lacking multiple class A high-molecular-weight penicillin-binding proteins. *J Bacteriol* **178:** 2079–2085.
Popham, D.L., Helin, J., Costello, C.E., and Setlow, P. (1996) Analysis of the peptidoglycan structure of *Bacillus subtilis* endospores. *J Bacteriol* **178:** 6451–6458.
Popham, D.L., Gilmore, M.E., and Setlow, P. (1999) Roles of low-molecular-weight penicillin-binding proteins in *Bacillus subtilis* spore peptidoglycan synthesis and spore properties. *J Bacteriol* **181:** 126–132.
Santo, L.Y., and Doi, R.H. (1974) Ultrastructural analysis during germination and outgrowth of *Bacillus subtilis* spores. *J Bacteriol* **120:** 475–481.
Sauvage, E., Kerff, F., Terrak, M., Ayala, J.A., and Charlier, P. (2008) The penicillin-binding proteins: structure and role in peptidoglycan biosynthesis. *FEMS Microbiol Rev* **32:** 234–258.
Scheffers, D.J. (2005) Dynamic localization of penicillin-binding proteins during spore development in *Bacillus subtilis*. *Microbiology* **151:** 999–1012.
Sekiguchi, J., Akeo, K., Yamamoto, H., Khasanov, F.K., Alonso, J.C., and Kuroda, A. (1995) Nucleotide sequence and regulation of a new putative cell wall hydrolase gene, *cwlD*, which affects germination in *Bacillus subtilis*. *J Bacteriol* **177:** 5582–5589.
Silhavy, T.J., Kahne, D., and Walker, S. (2010) The bacterial cell envelope. *Cold Spring Harb Perspect Biol* **2:** a000414.
Smith, K., Bayer, M.E., and Youngman, P. (1993) Physical and functional characterization of the *Bacillus subtilis spoIIM* gene. *J Bacteriol* **175:** 3607–3617.
Suloway, C., Pulokas, J., Fellmann, D., Cheng, A., Guerra, F., Quispe, J., *et al*. (2005) Automated molecular microscopy: the new Leginon system. *J Struct Biol* **151:** 41–60.
Thwaites, J.J., and Mendelson, N.H. (1991) Mechanical behaviour of bacterial cell walls. *Adv Microb Physiol* **32:** 173–222.
Tipper, D.J., and Linnett, P.E. (1976) Distribution of peptidoglycan synthetase activities between sporangia and forespores in sporulating cells of *Bacillus sphaericus*. *J Bacteriol* **126:** 213–221.
Tocheva, E.I., Li, Z., and Jensen, G.J. (2010) Electron cryotomography. *Cold Spring Harb Perspect Biol* **2:** a003442.
Tocheva, E.I., Matson, E.G., Morris, D.M., Moussavi, F., Leadbetter, J.R., and Jensen, G.J. (2011) Peptidoglycan remodeling and conversion of an inner membrane into an outer membrane during sporulation. *Cell* **146:** 799–812.
Todd, J.A., Roberts, A.N., Johnstone, K., Piggot, P.J., Winter, G., and Ellar, D.J. (1986) Reduced heat resistance of mutant spores after cloning and mutagenesis of the *Bacillus subtilis* gene encoding penicillin-binding protein 5. *J Bacteriol* **167:** 257–264.
Touhami, A., Jericho, M.H., and Beveridge, T.J. (2004) Atomic force microscopy of cell growth and division in *Staphylococcus aureus*. *J Bacteriol* **186:** 3286–3295.
Tuson, H.H., Auer, G.K., Renner, L.D., Hasebe, M., Tropini, C., Salick, M., *et al*. (2012) Measuring the stiffness of bacterial cells from growth rates in hydrogels of tunable elasticity. *Mol Microbiol* **84:** 874–891.
Typas, A., Banzhaf, M., Gross, C.A., and Vollmer, W. (2011) From the regulation of peptidoglycan synthesis to bacterial growth and morphology. *Nat Rev Microbiol* **10:** 123–136.
Vasudevan, P., Weaver, A., Reichert, E.D., Linnstaedt, S.D., and Popham, D.L. (2007) Spore cortex formation in *Bacillus subtilis* is regulated by accumulation of peptidoglycan precursors under the control of sigma K. *Mol Microbiol* **65:** 1582–1594.
Verwer, R.W., and Nanninga, N. (1976) Electron microscopy of isolated cell walls of *Bacillus subtilis* var. *niger*. *Arch Microbiol* **109:** 195–197.
Vollmer, W., Blanot, D., and de Pedro, M.A. (2008) Peptidoglycan structure and architecture. *FEMS Microbiol Rev* **32:** 149–167.
Zheng, S.Q., Keszthelyi, B., Branlund, E., Lyle, J.M., Braunfeld, M.B., Sedat, J.W., and Agard, D.A. (2007) UCSF tomography: an integrated software suite for real-time electron microscopic tomographic data collection, alignment, and reconstruction. *J Struct Biol* **157:** 138–147.

Supporting information

Additional supporting information may be found in the online version of this article at the publisher's web-site.